

# Friction Stir-Welded Titanium Alloy Ti-6Al-4V: Microstructure, Mechanical and Fracture Properties

D.G. SANDERS,<sup>1,2</sup> P. EDWARDS,<sup>1,2</sup> A.M. CANTRELL,<sup>1</sup> K. GANGWAR,<sup>1</sup> and M. RAMULU<sup>1,3,4</sup>

1.—Department of Mechanical Engineering, University of Washington, Seattle, WA, USA. 2.—The Boeing Company, Seattle, WA, USA. 3.—e-mail: ramulum@u.washington.edu. 4.—e-mail: ramulum@uw.edu

Friction stir welding (FSW) has been refined to create butt welds from two sheets of Ti-6Al-4V alloy to have an ultra-fine grain size. Weld specimen testing was completed for three different FSW process conditions: As welded, stress relieved, stress relieved and machined, and for the un-welded base material. The investigation includes macrostructure, microstructure, microhardness, tensile property testing, notched bar impact testing, and fracture toughness evaluations. All experiments were conducted in accordance with industry standard testing specifications. The microstructure in the weld nugget was found to consist of refined and distorted grains of alpha in a matrix of transformed beta containing acicular alpha. The enhanced fracture toughness of the welds is a result of increased hardness, which is attributed to an increase in alpha phase, increase in transformed beta in acicular alpha, and grain refinement during the weld process. The noted general trend in mechanical properties from as welded, to stress relieved, to stress relieved and machined conditions exhibited a decrease in ultimate tensile strength, and yield strength with a small increase in ductility and a significant increase in fracture toughness.

## INTRODUCTION

Friction stir welding (FSW), invented in 1991 at The Welding Institute in Cambridge, UK, is a solid-state joining process that utilizes friction between the material being joined, and a rotating non-consumable tool, in order to generate the needed heat to plasticize and mix the material.<sup>1–6</sup> FSW, in addition to producing strong<sup>6</sup> and more reliable welds, generates no fumes or splatter, creates far less distortion, and is more energy efficient as compared with traditional fusion welding processes. Fusion welding techniques melt the material, resulting in varying degrees of voids, defects, cracks and distortion associated with thermal contraction during cooling.<sup>1,4,6</sup> Furthermore, FSW can be used on thin sheets of material where making a fusion weld would be extremely difficult or even impossible. FSW geometries can include butt welds, overlap welds, T-sections and corner welds.<sup>1,5</sup>

Ti-6Al-4V is known as the workhorse of aerospace industry. In order to reduce the buy-to-fly ratio, which is used to describe the cost associated with the amount

of raw materials required to produce a finished part ratio, it is of paramount to produce as little scrap as possible. In the current study, experiments on FSW-ed sheets of Ti-6Al-4V have been carried out to relate the microstructural properties with microhardness and mechanical properties. In order to develop a production-hardened process for FSW of titanium and its alloys, the tool must be fabricated using an alloy with high compressive strength, good high temperature tensile strength, excellent high temperature hardness, exceptional toughness and high temperature oxidation resistance.<sup>7–13</sup> In addition to the importance of the rotating tool, new FSW machines need to be developed for the processing of titanium due to much higher loads and the need for less deflection of the machine frame during FSW processing.<sup>11–14</sup> Enabling this machine and tooling technology has so far proven to be difficult, but is currently possible at a handful of laboratories around the world.<sup>15–20</sup>

The titanium welds and superplastic-formed joint mechanical properties reported previously<sup>21–32</sup> were essential for variable FSW process conditions. Since

then, the process has been further developed and refined, and optimal process conditions for a given tool geometry have been identified.<sup>27</sup> Thus, it is of interest to repeat the mechanical tests performed in order to determine if the evolved processing techniques have in fact led to improved mechanical properties. To date, no evaluations have been performed on the fracture properties associated with impact testing and fracture toughness testing of Ti-6Al-4V FSW, which would be design drivers for incorporating the process into producing lower cost welded titanium structures. The purpose of this study is to conduct additional tests using the optimal FSW conditions, and evaluating not only mechanical properties but also the fracture properties of Ti-6Al-4V FSW butt joint.

## EXPERIMENTAL PROCEDURES

### Material

Ti-6Al-4V is alpha stabilized with 6% aluminum and beta stabilized with 4% vanadium. The base metal (BM) sheets used in this study were thermo-mechanically processed at the mill to have a grain size of 0.8–2  $\mu\text{m}$  and a nominal sheet thickness of 2.54 mm (0.100 inch). The fine grain Ti-6Al-4V sheet material was divided into sheets 610 mm long by 102 mm wide ( $\sim 16 \times 4$  inch). Two sectioned pieces of the sheet were tack welded together by laser fusion welding, placed on the friction stir anvil, and butt welded with 1.27 mm/s traverse speed and 300 rpm. To prevent oxidation, FSW was performed in the presence of argon gas. FSW of Ti-6Al-4V was conducted at the Boeing Research & Technology Welding Laboratory in Auburn, Washington, USA. The specimen preparation, mechanical testing and metallurgical evaluations were conducted in engineering laboratories at the University of Washington in Seattle, Washington, unless otherwise noted.

### Processing

The as-welded (AW) coupons were simply butt welded with no post-processing. Stress relieved (SR) specimens were stress relieved according to the industry standard (heat treated at 774°C for 45 min, and then air-cooled) in order to relieve the residual stresses. A post-process machining step (SR-M) was done to remove the surface roughness caused by the FSW pin tool swirl marks on the surface of the titanium sheet butt welds. In summary, the conditions tested in this study are as follows:

- Condition 1 Base material (BM)
- Condition 2 As welded (AW)
- Condition 3 As welded followed by a stress relief thermal cycle (SR)
- Condition 4 Machined and stress relieved (SR-M)

### Weld Microstructure and Hardness

Macrostructural evaluations were performed on transverse cross-sections of the FSWed specimen of

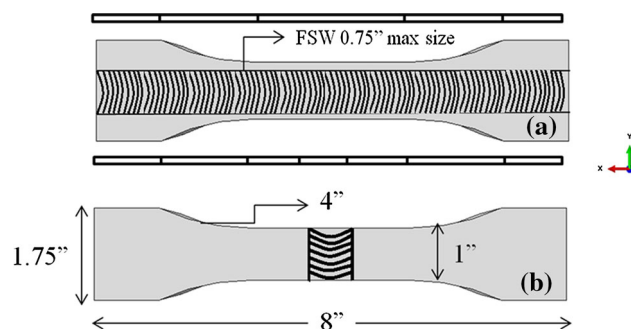


Fig. 1. Ti-6Al-4V FSW tensile specimen configurations. Longitudinal to FSW (a), transverse to FSW (b).

Ti-6Al-4V for the above-mentioned conditions. Each specimen was sectioned, mounted, and polished in accordance with ASTM E3-01, with special care in order to not alter the surface of the specimen. The mounted metallographic specimens were first etched with 2% HF etchant (as per ASTM E407-07) for macrostructure and microstructure and then re-polished for microhardness evaluation. Each microhardness (as per ASTM E384-06) profile consisted of 3 microhardness traverses with 100 indents each with a spacing of 254  $\mu\text{m}$  at a depth of 508  $\mu\text{m}$ , 1270  $\mu\text{m}$ , and 2032  $\mu\text{m}$  from the top. All the microhardness indent traverses were conducted on a LECO AMH43 Automatic Hardness Testing System using a Vickers indenter with a 500-g load. Additionally, using the combination of 3 traverses (hardness profiles) for each condition, the AMH43 software interface allowed us to create a color-coded mapping of hardness for each the weld cross-sections.

### Tension Testing

The tensile specimens were machined from FSW butt weld specimens with both transverse and longitudinal welds relative to the specimen length (Fig. 1). The tensile specimens were cut to shape with a 3-axis programmable abrasive waterjet system (WJP1313) at the University of Washington. A total of 12 tensile specimens, 2 specimens for each processing condition and weld direction, were tested in accordance with ASTM E8M-04 and AMS-T-9046B on an Instron<sup>TM</sup> test frame under displacement control monitored by a laser extensometer for determining the instantaneous strain rate. Fracture surfaces of the tensile specimens were also examined macroscopically and microscopically for failure mode and fracture initiation.

### Fracture Toughness Testing

Fracture toughness testing was performed using the R-curve method to determine the apparent fracture toughness of the SR welded joints. The R-curve method was used because the minimum thickness of material required for satisfying plane strain fracture toughness conditions. Compact tension specimen (CT) (Sheet thickness,  $B = 2.52 \pm$

0.02 mm), as described in the ASTM E561 test specification, was adopted in this study to ensure proper and accurate fracture toughness measurements of the FSW specimens. The specific location of the sample CT specimens relative to the FSW butt welds is shown in Fig. 2a. Given the location and direction of crack propagation for each CT specimen, 3 sample specimens were taken from each welded condition for each location described as in Fig. 2a. Each CT specimen was mounted on a low-speed saw and cut with a thin (less than 2 mm) diamond blade on both sides to make a chevron-shaped notch. This chevron notch not only insures pre-crack direction but also creates equilateral initialization of the crack front. CT test coupons were then mounted onto the compact loading clevis of an MTS test frame wedge grip setup using a double cantilever clip-in displacement gage. The 4-mm clip gage was placed in the notched area at the end of the mouth of the CT specimens. Before starting the fracture toughness load/displacement test a fatigue pre-crack of length  $0.025 W$  (or 1.3 mm) was required for the test method specifications used in this study. For every CT specimen, the crack mouth opening displacement (CMOD) was measured with a displacement gage along with the applied load using the load cell built into the load frame. From this load versus displacement data,  $K$  versus effective crack length curve was derived using the equations in accordance with ASTM E 561.

### Notched Impact Testing

Impact testing was conducted in accordance with ASTM E23 (Notched Bar Impact Test Methods) for two notch types, U-notch and V-notch (Charpy) specimens. A nominal thickness of 2.5 mm in the sheet material requires the use of the defined non-standard (sub-size) specimen configurations as per section A3 of ASTM E23. The specific notch type, locations, and directions of the sample impact specimens are shown in Fig. 2b.

A total of 8 samples (4 in each longitudinal and transverse direction) specimens were taken from both the AW and the SR welded conditions from the center of the weld. There were 7 sample specimens taken for BM, 4 in longitudinal and 3 in transverse to the rolling direction. Specimen trimming was completed using an Abrasive WaterJetPro System (WJP1313) and a v-notching tool bit using a Bridgeport milling machine. For impact testing the notching of the specimen not only ensured precise fracture direction or location but it also created a preferred initialization and propagation direction that helped to standardize the location of the fractures relative to the impact strike. Each specimen was then measured for thickness and width to ensure accurate measurement of the cross-sectional area. The impact testing procedure was then followed for each specimen, resulting in a specific absorbed impact energy measurement needed to

completely fracture each specimen. This procedure was conducted on an impact pendulum machine in accordance with Annex A1 of ASTM 23.

## RESULTS AND DISCUSSION

### Macro and Microstructure

The resulting macrographs of the FSW butt weld cross sections are shown in Fig. 3. Visually, it is apparent that there are no inclusions or voids revealed in the macros. The tool does not completely penetrate through the thickness of the weld in condition 2. Full penetration was not a requirement at this stage of the weld process development, but will be desired in the future. Thus, the lack of full penetration should be noted and this factor will be considered when observing the mechanical properties later in the study. However, the laser tack weld in the root provided full fusion of the joint in the absence of a full penetration weld nugget (WN). This visual contrast in the WN is due to the post process stress relief that had been conducted for SR, and SR-M conditions. Overall it can be noted that the visual weld quality is very good.

As shown in Fig. 4, the parent (base) material is composed of alpha phase with intergranular beta phase. The heat-affected zone (HAZ) is a transition of primary alpha with intergranular beta set within a matrix of alpha and intergranular beta that has smaller portions of acicular alpha intermixed. The location of the thermo mechanical affected zone (TMAZ), which lies between HAZ and WN, is not easily denoted because of its small size. The TMAZ microstructure is composed of a distorted matrix of alpha and intergranular beta with acicular alpha. The WN constitutes refined and distorted grains of alpha in a matrix of transformed beta containing acicular alpha (Fig. 4). The beta phase (dark), and alpha phase (light) is consistent with others.<sup>8-11,23,24</sup> Grain enlargement throughout the specimen and an increase of beta phase in the weld and HAZ of the joint can be observed in Fig. 4. Furthermore, elongated alpha grains in a matrix of beta can be seen in the SR and SR-M conditions base material. After the stress relieving, more acicular alpha grains, elongated however, have been observed in the transformed beta matrix. An additional machining has increased the amount of alpha phase at all the prescribed location as can be seen in the SR-M microstructure. In general, it can be observed that SR contains a higher percentage of alpha phase in the WN as compared with the WN in AW condition. The grains have also elongated after the post-welding processes due to the temperature increase followed by recrystallization. These observations were consistent with others.<sup>13,16,18,33,34</sup>

### Microhardness Distribution

The hardness profiles are shown in Fig. 5 where the changes in hardness across the transverse cross-section of the weld can be noticed at prescribed

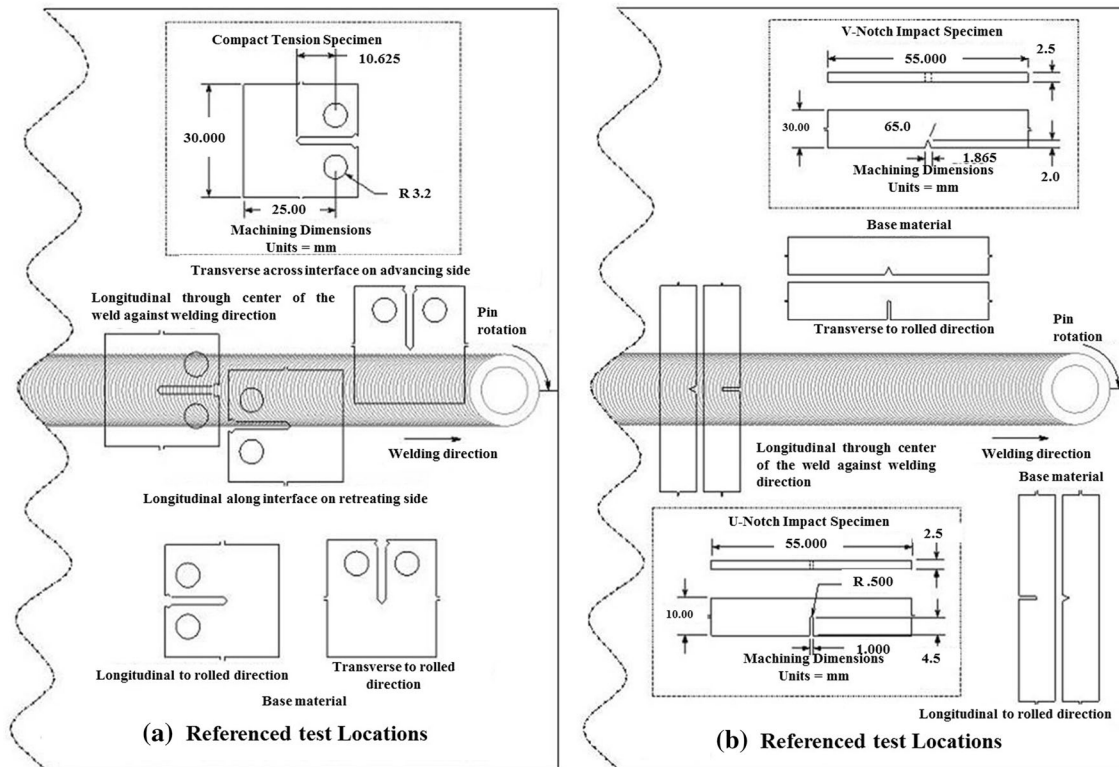


Fig. 2. CT specimen size and FSW location in the welded sheets (a), impact specimen size, type and locations in the FSW butt-welded test specimens (b).

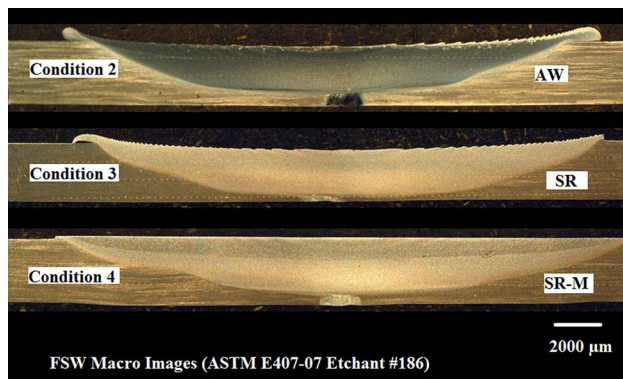


Fig. 3. Macrographs of FSW butt-joints for three different test conditions.

depths for AW, SR, and SR-M. Based on the observations, it can be concluded that the hardness decreased significantly from AW to SR. The average values of hardness along the three transverse depths for AW condition were 312, 315, and 319 HV in comparison with the average values of hardness, 303, 303, and 304 HV for SR condition along the similar transverse depths. As a result of machining, that affected only the surface layer (transverse 1), the hardness value of base materials has increased from 303 HV for SR to 313 HV for SR-M condition. Furthermore, the values of hardness in the WN for AW conditions vary roughly by about 5 HV for three

different transverse depths. However, for SR and SR-M, there is a significant change in the hardness values of WN for different transverse depths. For SR, the average values of hardness are 363, 358, and 342 HV, and for SR-M average values are 328, 328, and 314 HV for transverse depths of 508  $\mu\text{m}$ , 1270  $\mu\text{m}$ , and 2032  $\mu\text{m}$ , respectively, in the weld nugget. These results are consistent with Sander's work.<sup>22</sup> One exception would be Lienert's<sup>2</sup> comparison study with a rotation speed of 275 rpm, which shows a very high peak in hardness for the HAZ. In this case, the material shearing/stirring from the FSW pin could have resulted in a localized heat treatment and/or strain hardening effect in the HAZ.

### Tensile Properties

Typical stress strain plots are shown in Fig. 6a, which were generated from the load and deflection data of the welds. As shown in Fig. 6b, there is only a small difference in strength properties between transverse to longitudinal in the AW conditions. When comparing the results of longitudinal AW and SR condition, a notable decrease in ultimate tensile strength (UTS) and a slight increase in values of elastic modulus (E) of the welds are observable. When comparing the results of transverse AW and SR conditions, a general decrease in the values of E, yield strength (Y), and UTS has been noted.<sup>35,36</sup>

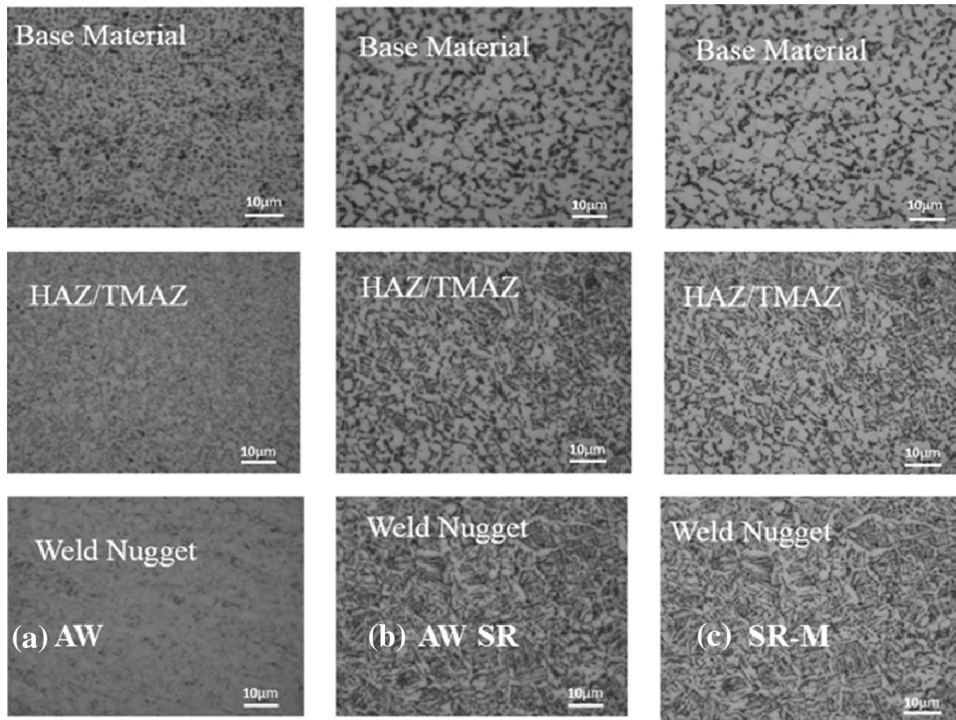


Fig. 4. Microstructure of the FSW zones for three different weld processing conditions shown at  $\times 1000$ . (a) W, (b) SR, (c) SR-M.

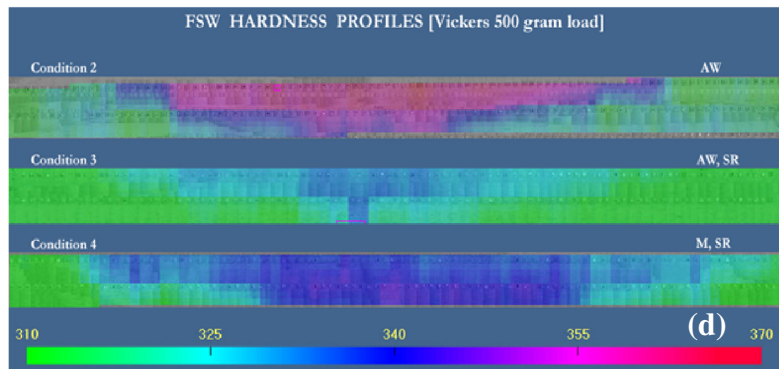
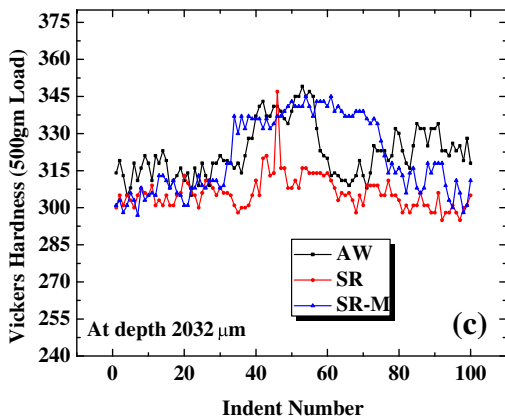
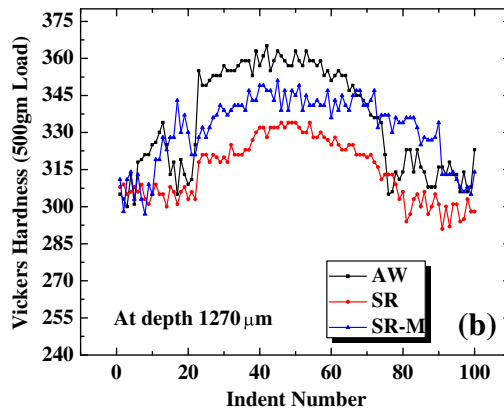
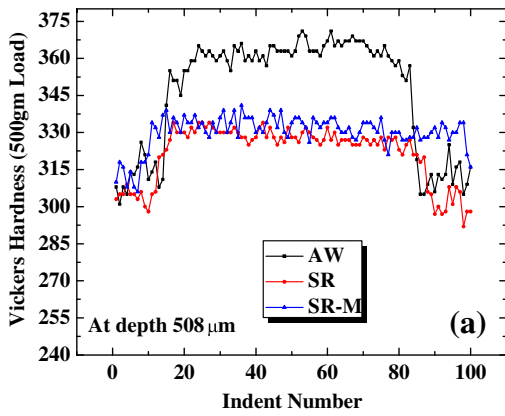


Fig. 5. Vickers hardness weld profiles at different depths across the transverse section of the weld, (a–c), and color coded hardness weld profiles (d).

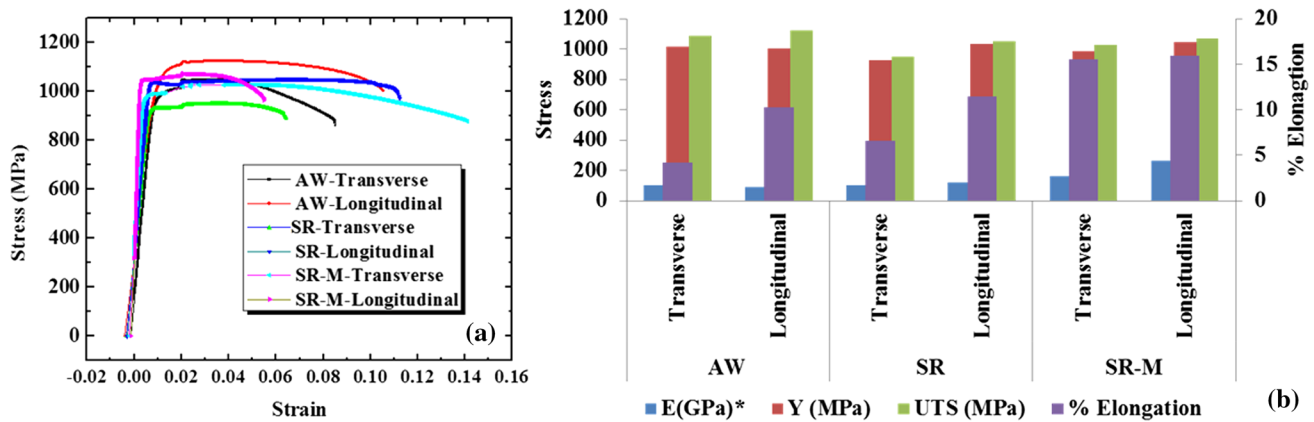


Fig. 6. Stress-strain curves for different conditions (a), and graphical representation of mechanical properties (b) (E is in GPa).

However, the ductility increases from AW to SR condition. The values of E, Y, and UTS and  $\epsilon$  increase from SR to SR-M in both longitudinal and transverse directions. Longitudinal welds show higher strength and ductility for SR, and SR-M condition. Almost all of the tensile properties in the FSW weld conditions were found to meet or exceed the mechanical requirements for standard BM (sheets of Ti-6Al-4V) for which the recorded values are: E, 113.8 GPa; Y, 1103 MPa; UTS, 1172 MPa; and the elongation at failure is about 10%.<sup>23,26,27</sup>

### Fracture Toughness

R-curves, or the resistance to crack extension, under Mode I loading for a given initial crack size were used to calculate the critical stress intensity factor. The purpose of the  $K_{Ic}$  result data is to account for the additional crack resistance due to residual stress imparted by the welding, and structural integrity at the joints. It can also be used to verify the fracture toughness of the weld specimen prepared under three different conditions. The weld center for the AW condition has lower fracture toughness as compared with SR and SR-M condition due to higher stress concentration. SR has a significant effect on the fracture toughness as can be noticed from Fig. 7. Fracture toughness values for AW and SR are in proximity of each other for the crack located at the weld interface on the advancing side. Nonetheless, machining also has a profound effect on the toughness values for the matching location of cracks at the weld interface. For the crack along HAZ, the fracture toughness values for AW condition are minimum among the three conditions, and the  $K_{Ic}$  values for SR, and SR-M conditions are nearly equal.

In summary, it can be said that AW and SR have similar effects on the fracture toughness values if the crack is barely in the proximity of welded region. Additionally, SR and SR-M have similar effects on the values of fracture toughness for as long as the crack has more spread or shares the maximum boundary with the welded region. It can be

said that fracture toughness in the FSWed Ti-6Al-4V sheet material varied with relative crack location and the weld zone. The values of fracture toughness are higher for the crack located along the interface and lower at the center of the weld. Furthermore, it can be added that fracture toughness increased with decreasing weld strength.

### Notched Impact Energy

The focus of the present study is to verify the change in the impact energy of Ti-6Al-4V butt weld from BM to AW, and to SR using two notch geometries. The results of the notched impact tests are shown in Fig. 8. The averages and standard deviations for each dataset are drawn from 6 test specimens.

Figure 8a shows the effect of size by comparing the impact energy of v-notch and u-notch. Decreasing the notch depth of the specimen enlarges the cross-sectional area subjected to distortion upon impact; this leads to an increase of energy absorption during the breaking of the specimen. The cross-sectional area that is subjected to distortion, for a uniform thickness of 2.5 mm, are: for v-notch, 12.5 mm<sup>2</sup>, and for u-notch, 20 mm<sup>2</sup>. Notch effect is also observed in Fig. 8b by comparing the impact energy per cross-sectional area of v-notch to u-notch. The sharper the notch, the lower the absorbed energy during impact. Simply stated, higher the stress concentration, the lower the resulting impact energy. Note that the energy per unit area of the u-notch is higher than the energy per unit area of the v-notch specimens. The radius of the u-notch is 1 mm compared to the 0.25 mm radius of the v-notch, thus a lower stress concentration factor for v-notch.

### Fractured Surfaces

The fractured surfaces of the tensile coupons were examined both visually and at  $\times 5$  magnification. Fractured surface macrographs were taken of each tested tensile specimen for all the three condition. Figure 9 shows an enlarged view of the tensile

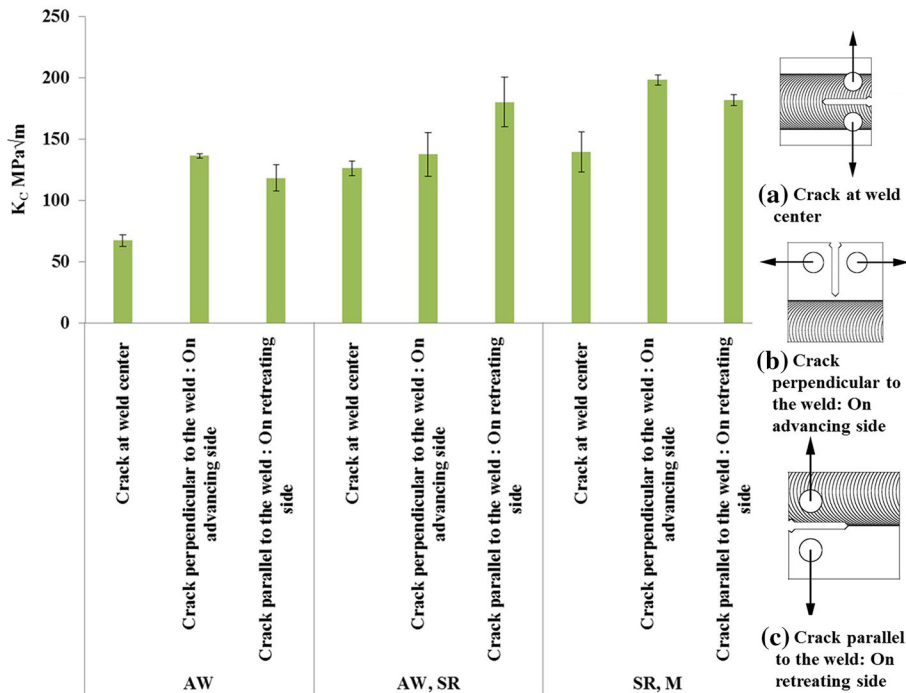


Fig. 7. Fracture toughness,  $K_c$ , for three different conditions.

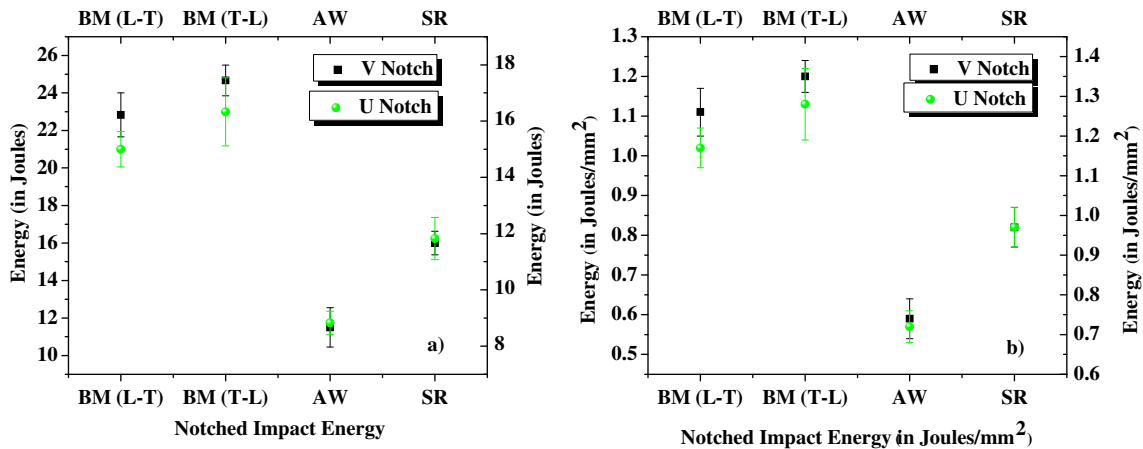


Fig. 8. Notched impact energy (a), and notched impact energy per cross-sectional area of the notch (b).

fractured specimens that correlates with the stress strain plots shown in Fig. 6a. It can be observed that in the AW transverse specimen fracture occurred in the base material on the retreating side of the FS weld. Note the large amount of local plastic yielding and cup and cone fracture behavior. This is typical of ductile material behavior. In contrast, the AW longitudinal specimen shows a ductile fracture with 45° shear plane. Both tested specimens' orientations for the SR condition have failed quite distinctly with less ductility. The fracture location of the transverse specimens of the SR-M condition occurred at the weld interface. There was a notable local plastic yielding on both the transverse and longitudinal specimens, resulting in an increase in

the percent of elongation and yield strength. In summary, the locations of tensile failure of FS welds are as follows: AW condition: BM; SR condition: WN; and SR-M: weld interface. From Fig. 9, it can be observed that the longitudinal tensile weld specimens are stronger than the transverse tensile weld specimen.

The fracture paths and surfaces of the AW transverse condition were documented using optical microscopy and SEM. Crack extensions and their paths reveal the consistency of the fracture behavior from crack location and weld condition. The fracture surfaces of CTS BM at two different orientations demonstrated that the preferred crack orientation is longitudinal to the rolling direction. The tested CTS

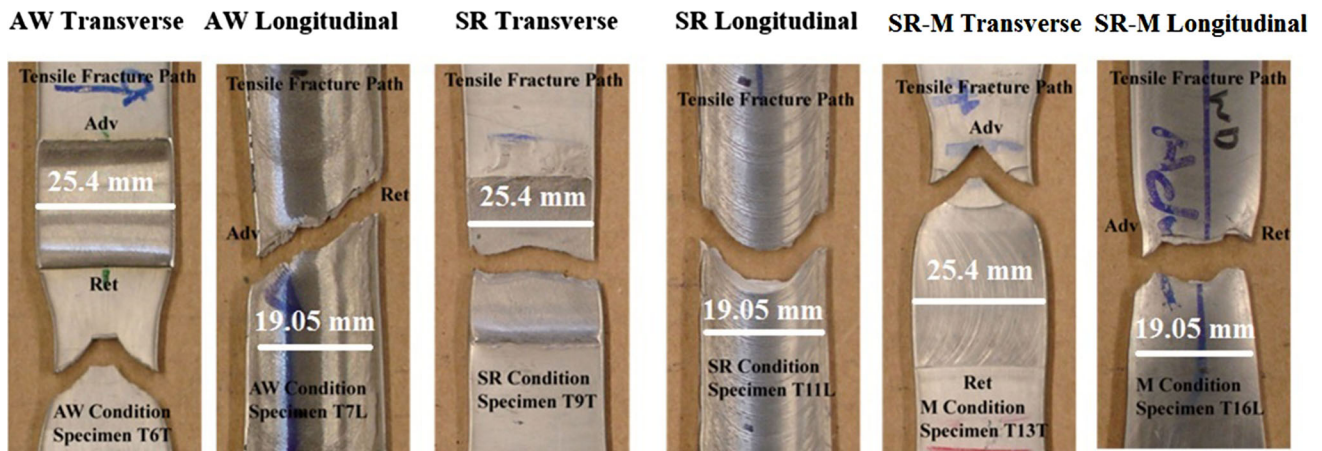


Fig. 9. Fractured test coupons for each process condition.

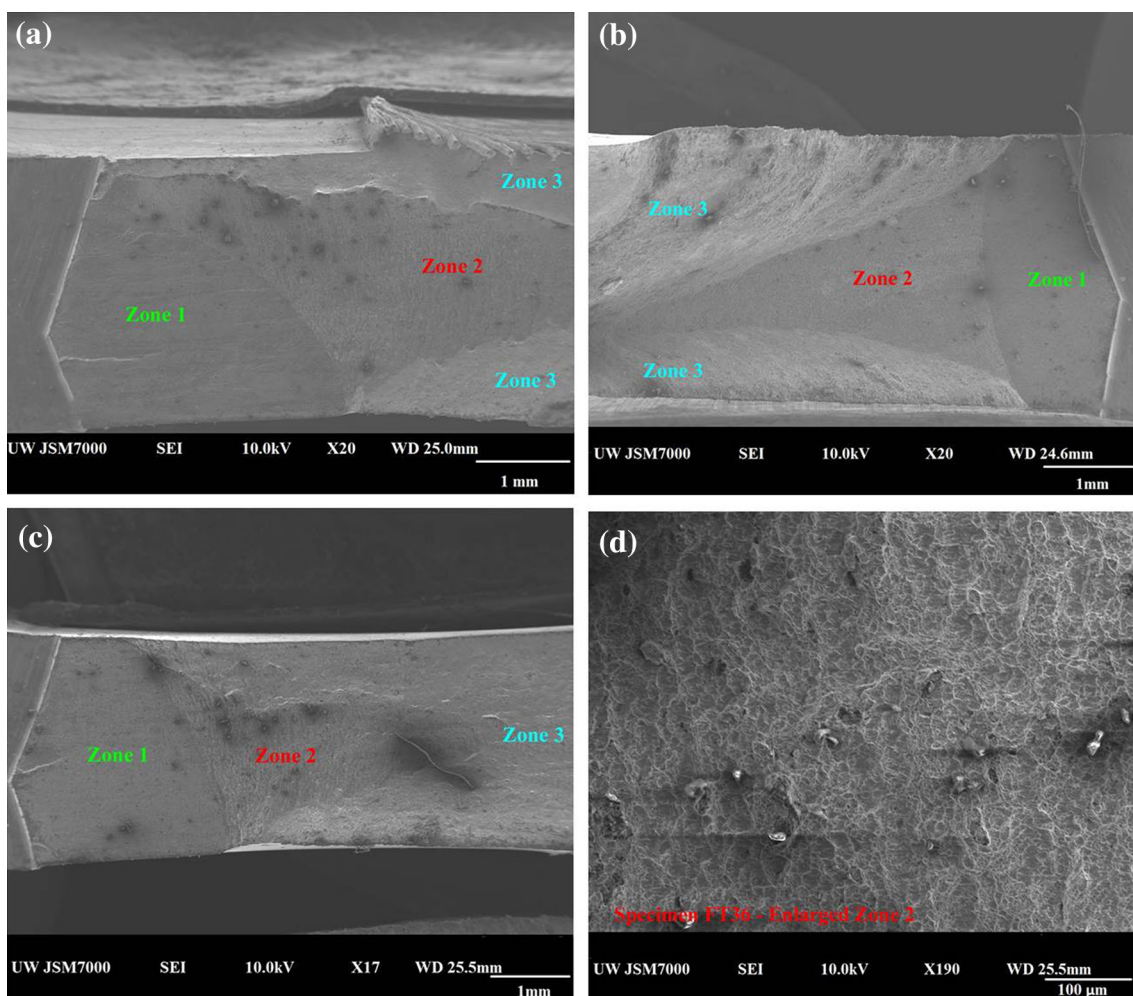


Fig. 10. SEM Images of fractured surfaces. Fatigue pre-cracking; AW transverse advancing side (a), crack blunting; SR-M longitudinal center (b), overload fracture; SR-M transverse advancing side (c), and crack blunting and initiation in zone 2; SR-M transverse advancing side (enlarged view), (d).

along the weld center showed the fracture path and fracture surfaces for the specimens where the crack is in the weld center for AW, SR, and SR-M, respectively. When considering the CTS in the center of the weld, the fracture paths/surfaces revealed low

ductility and brittle fracture in AW condition. However, an increased ductility and shear lip fracture is observed in SR-M condition. In the CTS that crossed the weld interface of the advancing side, we see an increasing ductile fracture across the weld



interface in the AW and SR condition, with a very brittle but slant fracture in the SR-M specimen. The CTS tested along the weld interface on the retreating side of the FS weld had brittle fractures with some notable pre-crack branching in the fatigue region of the AW and SR condition specimens.

The fracture path and surface of the tested CTS revealed three fracture zones: fatigue pre-cracking (zone 1), crack blunting (zone 2), and overload fracture (zone 3). Three fractured CTS were selected for SEM evaluation. The SEM images in Fig. 10 displays the three noted zones. An enlarged view of the crack blunting and initiation in zone 2 of specimen fracture toughness testing specimen is shown. The SEM image shows microvoid coalescence in the fracture surface that occurred during the crack extension under load. Microvoid coalescence involves nucleation, growth, and coalescence or joining of the formed voids.

### CONCLUSION

Based on the results obtained for butt welded Ti-6Al-4V fine grain sheet material for three different conditions, AW, SR, and SR-M, the following conclusions were drawn:

1. Macrostructures revealed a good quality weld joint with no inclusions, no voids, and complete fusion.
2. Microstructures were determined to be: BM composed of alpha phase with intergranular beta, bimodal structure; HAZ transition of the bimodal structure with smaller portions of acicular alpha intermixed; and WN constituted refined and distorted grains of alpha in a matrix of transformed beta containing acicular alpha. All confirmed that temperature during welding exceeded the beta transus temperature. Furthermore, the microstructure of the AW stir zone displayed high grain refinement, which increased with the depth of the weld. Upon thermal stress relief, all the microstructures throughout the weld received grain enlargement. The detailed visual color change revealed a large increase in alpha phase in the SR condition with a reduction of alpha and an increase in beta from the AW condition.
3. Microhardness of the BM decreased roughly by 10 HV due to the stress relief cycle. Machining on the other hand increased the BM hardness by 10 HV. There was a discrete change in the hardness values of the WN as a function of depth in the transverse direction of the weld. In the AW condition, the hardness values of WN changed by roughly 5 HV for each undertaken traverse depth. The stress relief cycle further reduced the hardness of the WN by approximately 30 HV.
4. Tensile properties. Mechanical properties from AW to SR conditions exhibited a decrease in UTS, and Y with a small increase in ductility in the longitudinal direction. Longitudinal weld specimens failed across the BM, HAZ, and WN in their gage cross-sections. The transverse weld specimens may fracture from any one of the edges of the weld and BM resulting in failure in its weakest component.
5. Fracture toughness. In the weld center for the SR condition, an increase in fracture toughness due to the stress relieving and machining has been observed. The results demonstrate higher fracture toughness in the weld zone interface than the WN center for all processing conditions. Weld interface results on the advancing side give a slight increase in fracture toughness as compared with the weld center in the SR condition.
6. Impact energy per unit area of the u-notch is higher than the energy per area of the v-notch specimens, and was always less than the base materials impact energy for fracture.

### ACKNOWLEDGEMENTS

The University of Washington acknowledges the support and cooperation of the Boeing Company during the course of this study.

### REFERENCES

1. R.S. Mishra and M.W. Mahoney: *Friction Stir Welding and Processing*, ed. (Materials Park, OH: ASM International, 2007).
2. T.J. Lienert: *Friction Stir Welding and Processing*, ed. (Materials Park, OH: ASM International, 2007), pp. 123–154.
3. P.D. Edwards and M. Ramulu, *Sci. Technol. Weld. Join.* 14, 775 (2009).
4. R. Nandan, T. DebRoy, and H.K.D.H. Bhadeshia, *Prog. Mater. Sci.* 53, 980 (2008).
5. D. Sanders, P. Edwards, G. Grant, M. Ramulu, and A.P. Reynolds, *EuroSPF* (France: Carcassonne, 2008).
6. R.S. Mishra and Z.Y. Ma, *Mater. Sci. Eng. R* 50, 1 (2005).
7. Y. Shang, Y.S. Sato, H. Kokawa, S.H.C. Park, and S. Hirano, *Mater. Sci. Eng. A* 488, 25 (2008).
8. W.B. Lee, C.Y. Lee, W.S. Chang, Y.M. Yeon, and S.B. Jung, *Mater. Lett.* 59, 3315 (2005).
9. A.L. Pilchak, M.C. Juhas, and J.C. Williams, *Metall. Mater. Trans.* 38A, 401 (2007).
10. A.L. Pilchak, D.M. Norfleet, M.C. Juhas, and J.C. Williams, *Metall. Mater. Trans.* 39A, 1519 (2008).
11. S. Mironov, Y. Zhang, and Y.S. Sato, H. Kokawa. *Scripta Mater.* 59, 27 (2008).
12. S. Mironov, Y. Zhang, and Y.S. Sato, H. Kokawa. *Scripta Mater.* 59, 511 (2008).
13. A. Lauro, *Weld. Int.* 26, 8 (2012).
14. S. Pasta and A.P. Reynolds, *Fatigue Fract. Eng. Mater. Struct.* 31, 569 (2008).
15. Y. Zhang, Y.S. Sato, H. Kokawa, S.H.C. Park, and S. Hirano, *Mater. Sci. Eng. A* 485, 448 (2008).
16. L. Zhou, H.J. Liu, and Q.W. Liu, *J. Mater. Sci. (Netherlands)* 45, 39 (2010).
17. L. Zhou, H.J. Liu, and Q.W. Liu, *Mater. Des.* 31, 2631 (2010).
18. H.J. Liu, L. Zhou, and Q.W. Liu, *Mater. Des.* 31, 1650 (2010).
19. H. Liu, K. Nakata, N. Yamamoto, and J. Liao, *Sci. Technol. Weld. Join.* 15, 428 (2010).
20. P.D. Edwards and M. Ramulu, *Int. J. Fatigue* 70, 171 (2015).
21. D.G. Sanders, M. Ramulu, E.J. Klock-McCook, P.D. Edwards, A.P. Reynolds, T. Trapp: *AeroMat Conference, International Symposium on Superplasticity and Superplastic Forming (SPF)*, Baltimore, MD 2007.
22. D.G. Sanders: 2007, Development of Friction Stir Welding Combined with Superplastic Forming Processes for the

- Fabrication of Titanium Structures. PhD Dissertation, University of Washington, Seattle, WA.
23. E.J. Klock-McCook: Characterization of Friction Stir Welded and Superplastically Formed Friction Stir Welded Joints of Titanium. Masters Thesis, University of Washington, Seattle, WA.
  24. P.D. Edwards: Experimental and Numerical Characterization of Friction Stir Welded and Superplastically Formed—Friction Stir Welded Titanium. Masters Thesis, University of Washington, Seattle, WA.
  25. M. Ramulu, P. Labossiere, and T. Greenwell, *Opt. Lasers Eng.* 48, 385 (2010).
  26. M. Ramulu, P. Labossiere, and T. Greenwell, *Appl. Mech. Mater.* 692, 490 (2014).
  27. P.D. Edwards and M. Ramulu, *J. Eng. Mater. Technol.* 132, 0310061 (2010).
  28. P.D. Edwards, D.G. Sanders, and M. Ramulu, *J. Mater. Eng. Perform.* 19, 510 (2010).
  29. D.G. Sanders, M. Ramulu, P.D. Edwards, and A. Cantrell, *J. Mater. Eng. Perform.* 19, 503 (2010).
  30. P.D. Edwards, D.G. Sanders, M. Ramulu, G. Grant, T. Trapp, and P. Comley, *J. Mater. Eng. Perform.* 19, 481 (2010).
  31. P. Edwards, M. Ramulu, and D. Sanders, *Key Eng. Mater.* 433, 169 (2010).
  32. G.D. Sanders and M. Ramulu, *Mater. Sci. Forum* 735, 395 (2013).
  33. R.W. Fonda and K.E. Knipling, *Acta Mater.* 58, 6452 (2010).
  34. N. Kulkarni and M. Ramulu: *Proceedings of the ASME2014 International Mechanical Engineering Congress & Exposition (IMECE2014), Montreal, 2014*, Paper # IMECE2014-39211.
  35. M.J. Donachie, Jr.: *Titanium and Titanium Alloys* ed. (Materials Park, OH: American Society for Metals, 1982).
  36. Material Property Data, March, 2009, <http://asm.matweb.com/search/SpecificMaterial.asp?bassnum=MTP641>.